Supplement of
Dominant contribution of oxygenated organic aerosol to haze particles from real-time observation in Singapore during an Indonesian wildfire event in 2015

Sri Hapsari Budisulistiorini [1], Matthieu Riva [2,#], Michael Williams [2], Takuma Miyakawa [3], Jing Chen [1], Masayuki Itoh [4], Jason D. Surratt [2], Mikinori Kuwata[1,4,5]

[1]Earth Observatory of Singapore, Nanyang Technological University, Singapore 639798, Singapore
[2]Department of Environmental Sciences and Engineering, Gillings School of Global Public Health, The University of North Carolina at Chapel Hill, Chapel Hill, North Carolina 27599, United States of America
[3]Research and Development Center for Global Change, Japan Agency for Marine-Earth Science and Technology, Kanagawa 236-0001, Japan
[4]Center for Southeast Asian Studies, Kyoto University, Kyoto 6068501, Japan
[5]Campus for Research Excellence and Technological Enterprise (CREATE), Singapore 138602, Singapore
[#]Now at the Univ Lyon, Université Claude Bernard Lyon 1, CNRS, IRCELYON, F-69626, Villeurbanne, France

Correspondence to: S. H. Budisulistiorini (sri.hb@ntu.edu.sg); M. Kuwata (kuwata@ntu.edu.sg)

Number of pages: 21
Number of tables: 8
Number of figures: 14

A. Comparison of total fine aerosol mass measurements

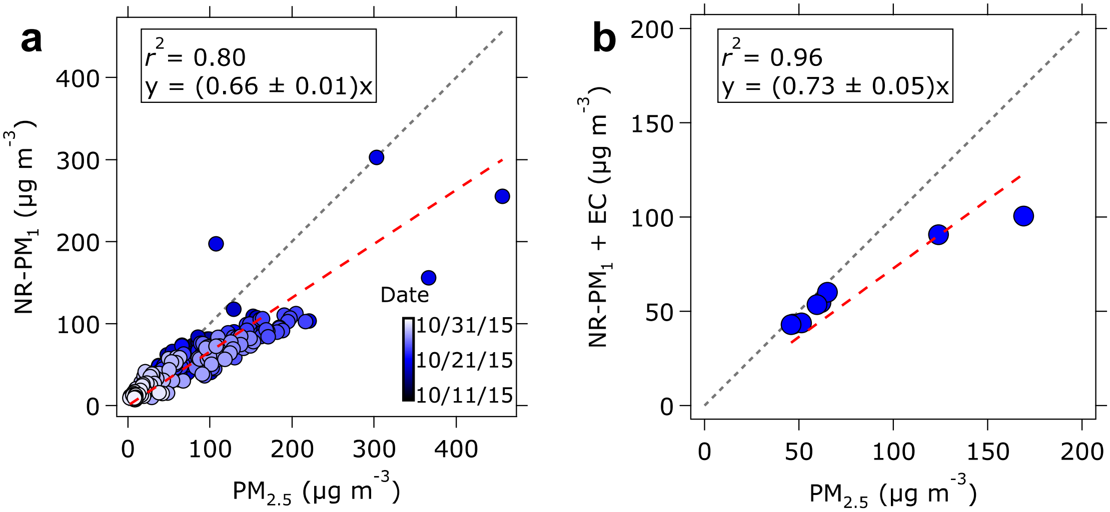

Figure S1: Linear regression plot of (a) NR-PM$_1$ mass concentration measured by ToF-ACSM and (b) estimated PM$_1$ mass concentration (as sum of NR-PM$_1$ and EC quantified from integrated samples) versus PM$_{2.5}$ mass concentration as reported in the website of the National Environment Agency (NEA) of Singapore. Contribution of EC to PM$_1$ is estimated to be around 9% during the entire campaign.

B. ME-2 Analysis

The unconstrained model yielded four-factor solution as shown in Fig. S2. Correlations of these four factors with the reference mass spectra (e.g., Ng et al., 2011), suggest that Factor 1 and 2 are hydrocarbon-like organic aerosol (HOA) and biomass burning organic aerosol (BBOA), respectively. The mass spectra of Factor 3 and 4, which both have good correlations with the reference low-volatility oxygenated organic aerosol (LV-OOA) factor (e.g., Ng et al., 2011), seem very similar to each other (R^2 ~0.9; Table S1). The similarities between Factor 3, and 4, indicate mixed factors. To further identify the factor solution, we constrained HOA and BBOA mass spectra in the ME-2 analysis. In addition, we constrained peat burning aerosol profile using mass spectrum from ToF-ACSM measurements of laboratory peat burning experiment (Budisulistiorini et al., 2017). We did not constrain OOA components and left it as the additional unconstrained factors (Crippa et al., 2014). The solutions were constrained with a-value between 0 and 0.3 (delta 0.05) and estimated for one to eight numbers of factors. The solutions were evaluated by comparing the variations of factor contribution to OA and the Q/Q_{exp} as functions of a number of factors per a-value. As illustrated in Fig. S3, the Q/Q_{exp} decreases with the number of factor solution, especially between one to four-factor solutions. Model solutions with more than four factors have less variation in the Q/Q_{exp} suggesting insignificant improvement in model solution. Hence, we selected four-factor solution as the optimum solution. Within the four-factor solution, a-value was selected to be the optimum variation based on factors correlation with external tracers as shown in Fig. S4 and Tables S2-S4.

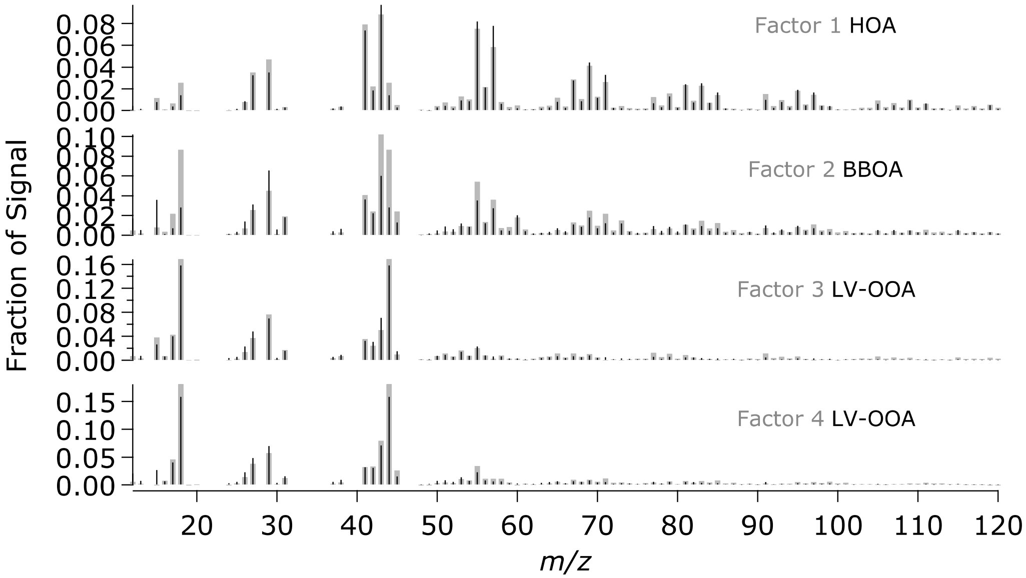

Figure S2: Mass spectra of factor solution from unconstrained model. Black bars are the reference mass spectra from AMS measurements at urban sites (Ng et al., 2011).

Table S1: Internal correlations of mass spectra (R_{MS}^2) and time series (R_{TS}^2) of factor solution from unconstrained model.

R_{MS}^2	Factor 1	Factor 2	Factor 3	Factor 4
Factor 1	1.00	0.59	0.16	0.20
Factor 2		1.00	0.65	0.76
Factor 3			1.00	0.94
Factor 4				1.00
R_{TS}^2				
Factor 1	1.00	0.54	0.23	0.00
Factor 2		1.00	0.78	0.18
Factor 3			1.00	0.22
Factor 4				1.00

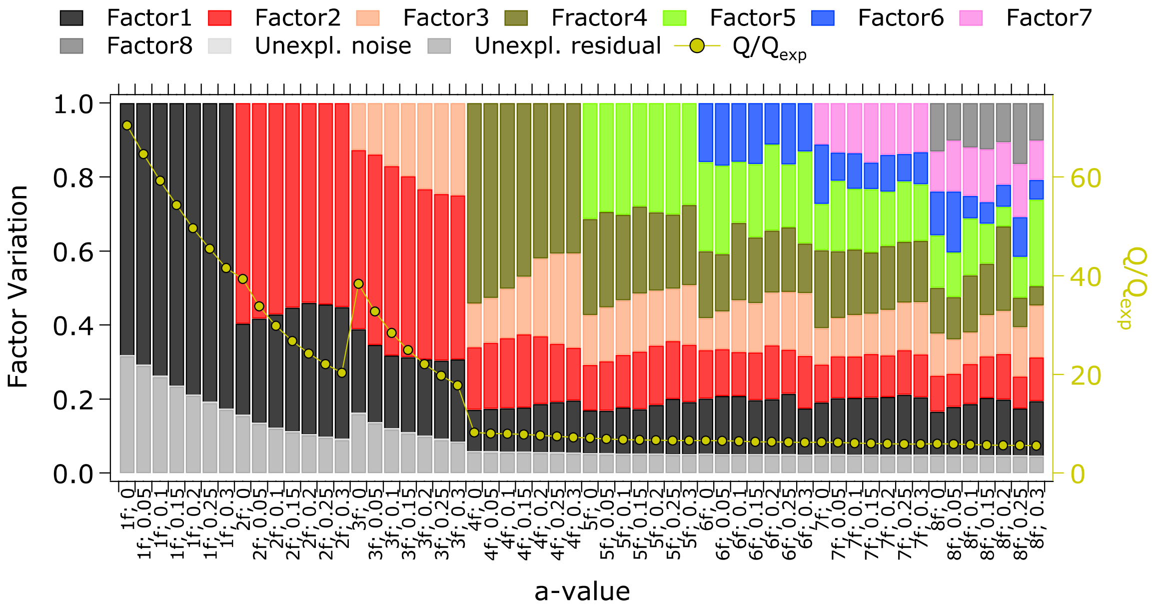

Figure S3: Variation of factor time series contribution (left axis) and Q/Q_{exp} parameter values across different model solutions (right axis) are plotted as functions of the number of factors and constraint parameter (a-value). Example of x-axis label, *4f;0.05* means four number of factors (4 factor solution) with a-value of 0.05 (5% deviation from reference).

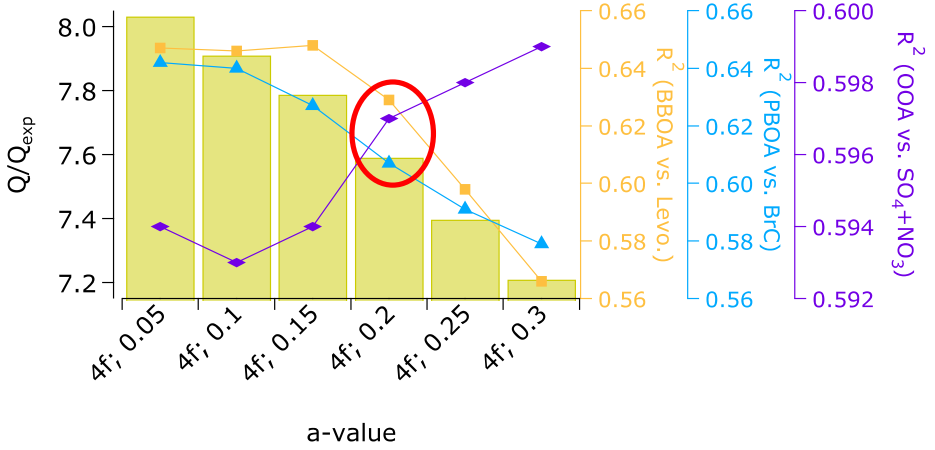

Figure S4: Q/Q_{exp} **(left axis) as a function of the best solution (4 factor solution) for each** a**-value. Coefficient of determination (**R^2**) of BBOA versus Levoglucosan, PBOA versus sum of brown carbon (BrC) tracers, and OOA and sum of** SO_4 **and** NO_3 **are plotted in the right axis.**

5

Table S2: Internal correlation of mass spectra (R_{MS}^2**) and time series (**R_{TS}^2**) of factor solution from the constrained model.**

R_{MS}^2	**HOA**	**BBOA**	**PBOA**	**OOA**
HOA	1.00	0.54	0.86	0.13
BBOA		1.00	0.45	0.35
PBOA			1.00	0.08
OOA				1.00
R_{TS}^2				
HOA	1.00	0.12	0.48	0.18
BBOA		1.00	0.63	0.81
PBOA			1.00	0.79
OOA				1.00

Table S3: Correlation between mass spectra of factor solutions of this study and references from previous studies.

R_{MS}^2	**HOA**	**BBOA**	**PBOA**	**OOA**	**Ref.**
HOA	0.97	0.46	0.91	0.11	a
LV-OOA	0.14	0.45	0.07	0.96	a
SV-OOA	0.60	0.80	0.55	0.46	a
BBOA	0.62	0.96	0.56	0.31	a

R_{MS}^2	HOA	BBOA	PBOA	OOA	Ref.
91Fac (Borneo)	0.81	0.75	0.65	0.52	b
Lab ISOPOOH SOA	0.75	0.85	0.67	0.15	c
IEPOX-OA (ATL 2012)	0.21	0.60	0.15	0.87	d
IEPOX-OA (ATL 2011)	0.29	0.69	0.22	0.67	e
IEPOX-OA (LRK 2013)	0.15	0.53	0.07	0.91	f
COA	0.86	0.57	0.68	0.11	g
PBOA	0.88	0.50	0.97	0.08	h
Lab IEPOX SOA	0.34	0.77	0.21	0.32	e

References: (a) Ng et al. (2011), (b) Robinson et al. (2011), (c) Riva et al. (2016), (d) Budisulistiorini et al. (2016), (e) Budisulistiorini et al. (2013), (f) Budisulistiorini et al. (2015), (g) Crippa et al. (2013), (h) Budisulistiorini et al. (2017).

5 **Table S4: Correlation between time trends of factor solution and chemical species quantified from offline (integrated samples) and online (real-time) measurements.**

R_{TS}^2	HOA	BBOA	PBOA	OOA	Ref.
Offline measurements					
Levoglucosan	0.24	0.63	0.69	0.63	a
Brown carbon	0.53	0.38	0.61	0.49	b
Isoprene SOA	0.02	0.00	0.00	0.00	c
Organosulfates	0.10	0.05	0.03	0.02	d, e
EC	0.00	0.07	0.04	0.08	
Inorganic cations					f
K^+	0.30	0.13	0.27	0.33	
Na^+	0.31	0.01	0.11	0.11	
Mg^{2+}	0.41	0.24	0.46	0.45	
Ca^{2+}	0.29	0.54	0.64	0.69	
Online measurements					
NH_4^+	0.16	0.42	0.53	0.63	
SO_4^{2-}	0.05	0.31	0.34	0.46	
NO_3^-	0.33	0.21	0.35	0.32	

R_{TS}^2	**HOA**	**BBOA**	**PBOA**	**OOA**	**Ref.**
$SO_4^{2-} + NO_3^-$	0.17	0.40	0.49	0.60	
Gaseous measurements					
CO	0.16	0.23	0.38	0.42	
NO_2	0.02	0.00	0.00	0.00	
O_3	0.04	0.05	0.02	0.08	

References: (a) Simoneit et al. (1999), (b) Budisulistiorini et al. (2017), (c) Surratt et al. (2007), (d) Ma et al. (2014), (e) Riva et al. (2016), (f) Cheng et al. (2013).

C. Filter Analysis

Table S5: Standards used for quantification of OA tracers by UPLC/DAD-ESI-HR-QTOFMS

Compound	**Formula**	**Remarks**
Organosulfates		
Sodium propyl sulfate	$C_3H_7O_4SNa$	commercial
Sodium octyl sulfate	$C_8H_{17}O_4SNa$	commercial
Authentic organosulfates		
2-methyltetrol sulfate	$C_5H_{12}O_7S$	synthesized at UNC CH
Nitroaromatics		
2-Nitrophenol	$C_6H_5NO_3$	commercial
4-Nitrophenol	$C_6H_5NO_3$	commercial
4-Nitrocatechol	$C_6H_5NO_4$	commercial
4-Nitro-o-cresol	$C_7H_7NO_3$	commercial
2-hydroxy-5-nitrobenzyl alcohol (HNBAL)	$C_7H_7NO_4$	commercial
2-Methyl-4-Nitroresorcinol (MNRC)	$C_7H_7NO_4$	commercial
2-Hydroxy-5-nitrobenzoic acid (HNBAC)	$C_7H_5NO_5$	commercial
2-methyl-4,6-dinitrophenol (MDNP)	$C_7H_6N_2O_5$	commercial
2,6-Dimethyl-4-nitrophenol (DMNP)	$C_8H_9NO_3$	commercial
4-Nitro-1-naphthol (NNAP)	$C_{10}H_7NO_3$	commercial

Table S6: Standards used in quantification of OA tracers by GC/EI-MS

Compound	**Formula**	**Remarks**
Anhydro sugars		
Levoglucosan	$C_6H_{10}O_5$	commercial
Mannosan	$C_6H_{10}O_5$	commercial
Authentic SOA		
2-methyltetrols	$C_5H_{11}O_4$	synthesized at UNC CH
Organic Acids		
Malic acid	$C_4H_6O_5$	commercial
Pimelic acid	$C_7H_{12}O_4$	commercial
Phthalic acid	$C_8H_6O_4$	commercial
Succinic acid	$C_4H_6O_4$	commercial

Compound	**Formula**	**Remarks**
Maleic acid	$C_4H_4O_4$	commercial
Adipic acid	$C_6H_{10}O_4$	commercial
Glutaric acid	$C_5H_8O_4$	commercial
Other		
Sucrose	$C_{12}H_{22}O_{11}$	commercial

D. Air Masses Backtrajectory

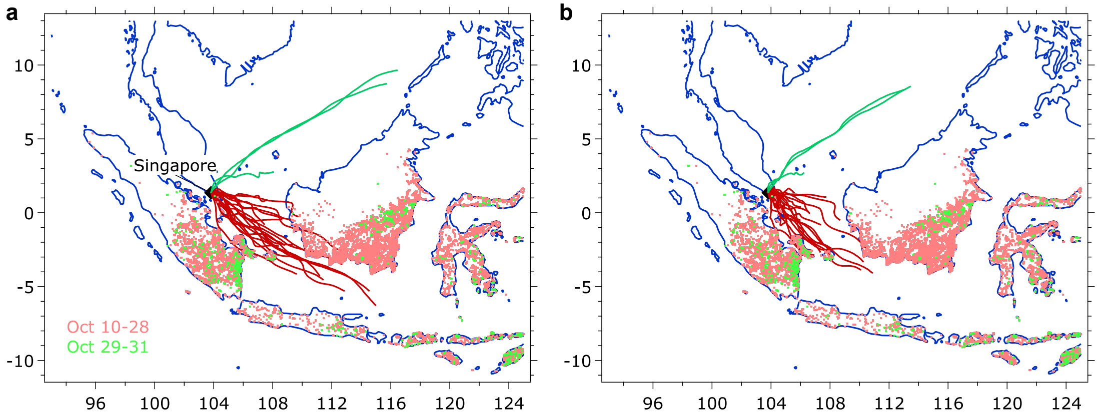

Figure S5: Air masses back-trajectory (NOAA Hysplit) at (a) 500 m and (b) 200 m above ground level (a.g.l.) at duration of 72 hour in Singapore between October 10 and 31, 2015. Fire hotspots in Indonesia as observed by NASA Terra/Aqua MODIS are plotted as dot markers colored in light-red for October 10-28 period and light-green for October 29-31 period. During October 10 to 28, the air masses mainly came from south and southeast (Sumatra and Kalimantan). This period was assigned as Period 1 (red lines). During October 29 to 31, the air masses mainly came from north and northwest (Malaysia and South China Sea). This period was assigned as Period 2 (green lines).

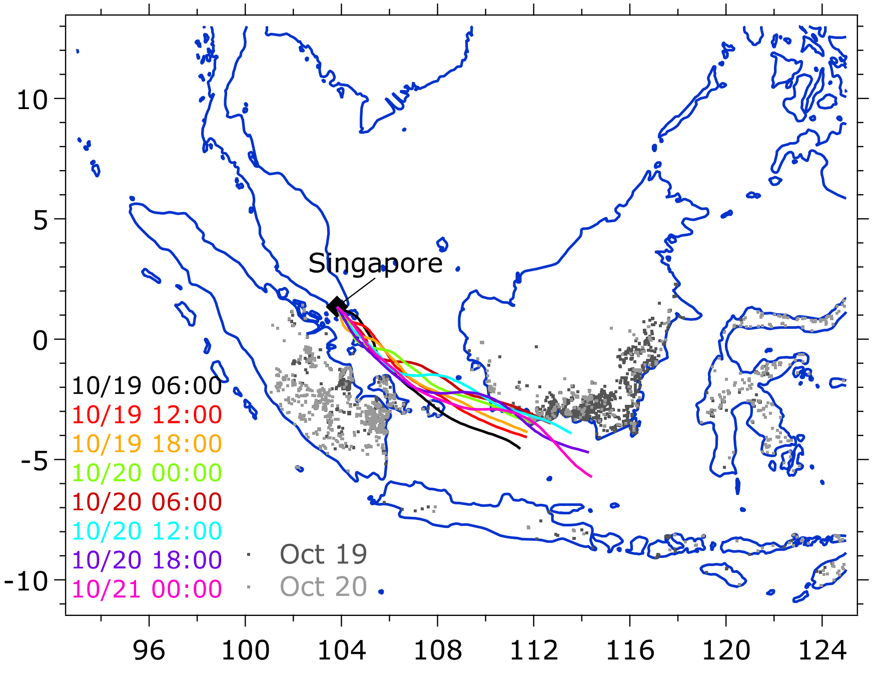

Figure S6: Air masses at 500 m a.g.l. in Singapore were estimated for four time periods of a day, i.e., 06:00, 12:00. 18:00, and 00:00 Local Time. Fire hotspots in Indonesia as observed by NASA Terra/Aqua MODIS are plotted as dot markers colored in light-red for October 10-28 period and light-green for October 29-31 period.

E. Elemental Analysis

Table S7: Descriptions of peat and vegetation analyzed by the Elemental Analyzer. Most of these samples were previously used in burning experiments which results have been reported by Budisulistiorini et al. (2017).

No.	Type	Name	Location	Description
1	Peat	Riau 1.1	Riau Province	Drained and burned peat
2	Peat	Riau 1.2	Riau Province	Drained and burned peat
3	Fern	Fern 1.1	Riau Province	Species: *Pteridium*. Dried fern.
4	Fern	Fern 1.2	Riau Province	Species: *Stenochlaena palustris*. Dried fern.
5	Leaf	Leaf	Riau Province	Species: *Acacia mangium* (acacia tree). Dried leaf.
6	Peat	CK 1.1	Central Kalimantan Province, Palangkaraya City	Drained and burned peat
7	Peat	CK 1.2	Central Kalimantan Province, Palangkaraya City	Drained and unburned peat
8	Peat	Riau 2	Riau Province	Unburned peat
9	Peat	Riau 3.1	Riau Province	Unburned peat
10	Peat	Riau 3.2	Riau Province	Unburned peat
11	Peat	Riau 3.2	Riau Province	Unburned peat

Note: Samples were collected at ground surface (within 0 – 10 cm depth).

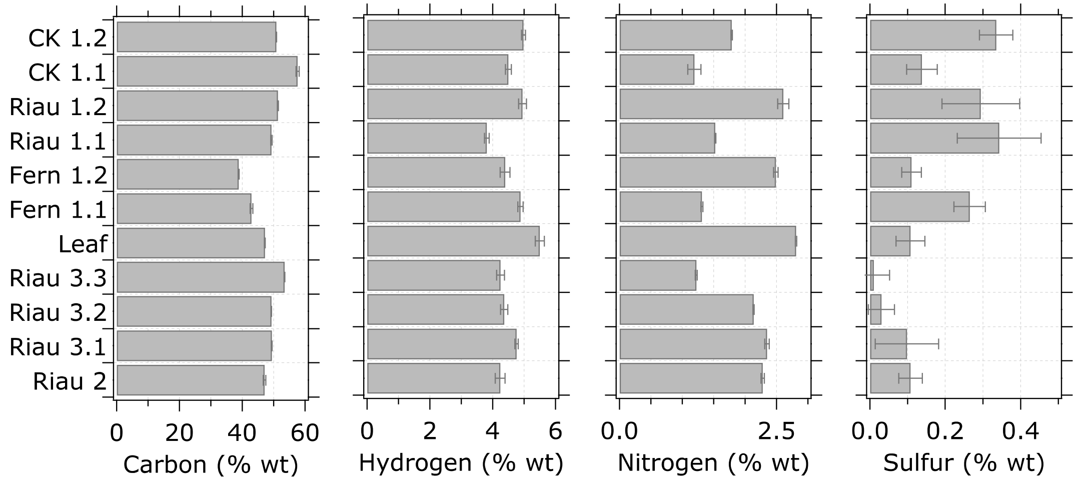

Figure S7: Carbon, hydrogen, nitrogen, and sulfur contents in percentage of the total sample weight.

F. Ambient Particle acidity

Ambient particle acidity was investigated by calculating neutralization degree of aerosol (Zhang et al., 2007). Neutralization degree of aerosol was calculated by the following equation:

$$\frac{NH_{4\,meas}^{+}}{NH_{4\,neu}^{+}} = \frac{[NH_4^+]}{2[SO_4^{2-}] + [NO_3^-] + [Cl^-]}$$

where $NH_4^+{}_{meas}$ (nmol m^{-3}) is the measured NH_4^+ and $NH_4^+{}_{neu}$ (nmol m^{-3}) is the NH_4^+ concentration required for full neutralization of the anions. Table S8 shows the estimated neutralization degree of aerosol during overall (October 10-31), P1 (October 10-28), and P2 (October 29-31) periods. Overall during the 2015 haze episode, NH_4^+ were in excess for neutralization of the anions as indicated by $NH_4^+{}_{meas}/NH_4^+{}_{neu}$ ratio equals to 0.9 ± 0.2. However, this estimation does not consider contribution of water to particle acidity.

Thermodynamic model ISORROPIA-II was used to estimate aerosol pH (Fountoukis and Nenes, 2007). Inputs for the model include aerosol-phase sulfate, nitrate, and ammonium in μmol m^{-3} , measured by the ACSM under ambient conditions, and RH and temperature obtained measured at NTU campus. ISORROPIA-II predicted particle hydronium ion concentration per volume of air (H^+_{air}, μg m^{-3}), liquid water content (LWC, μg m^{-3}), and aerosol aqueous phase mass concentration (μg m^{-3}). Aerosol pH is calculated by the following equation:

$$pH = -\log_{10} a_{H^+} = -\log_{10}\left(\frac{H_{air}^{+}}{LMASS} \times \rho_{aer} \times 1000\right)$$

where is H^+ activity in aqueous phase (mol L^{-1}), *LMASS* is the total liquid-phase aerosol mass (μg m^{-3}) and is aerosol density (g cm^{-3}). It should be noted that contribution of NH_3 and organic water were not included in the calculation due to unavailability of gas-phase NH_3 and organic aerosol water measurements.

Table S8: Average, standard deviation (SD), minimum and maximum values of ratio of measured ammonium concentration ($NH_4^+{}_{meas}$) to concentration of ammonium needed to fully neutralized the anions ($NH_4^+{}_{neu}$).

	Overall	P1	P2
mean	0.9	1.0	0.7
1 SD	0.2	0.1	0.3
minimum	0.0	0.0	0.0
maximum	1.9	1.7	1.9

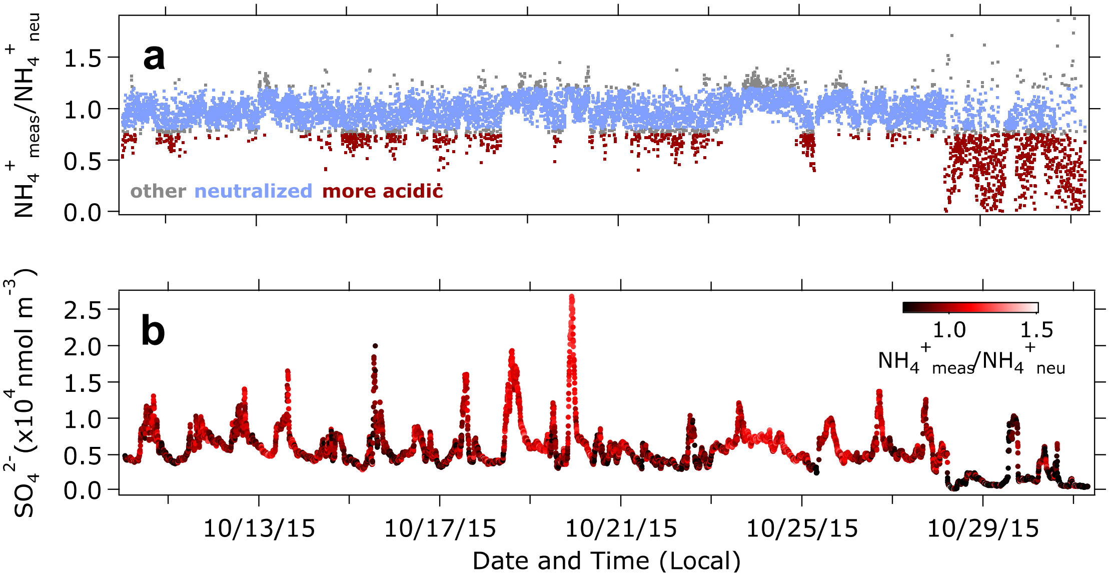

Figure S8: Time series of (a) $NH_4^+{}_{meas}$/ $NH_4^+{}_{neu}$ ratio and (b) sulfate concentration (bottom) in submicron particles. $NH_4^+{}_{meas}$/ $NH_4^+{}_{neu}$ ratio equals to 1 ± SD indicates that cations and anions are in a balance, whereas less than 0.75 indicates more acidic particles (Zhang et al., 2007).

5

Table S9: Average, standard deviation (SD), minimum and maximum values of aerosol acidity (pH) estimated by ISORROPIA-II.

	Overall	P1	P2
mean	1.2	1.3	0.6
1 SD	0.6	0.6	0.6
minimum	-0.6	-0.3	-0.6
maximum	2.5	2.5	2.1

G. Chemical Species Characterization

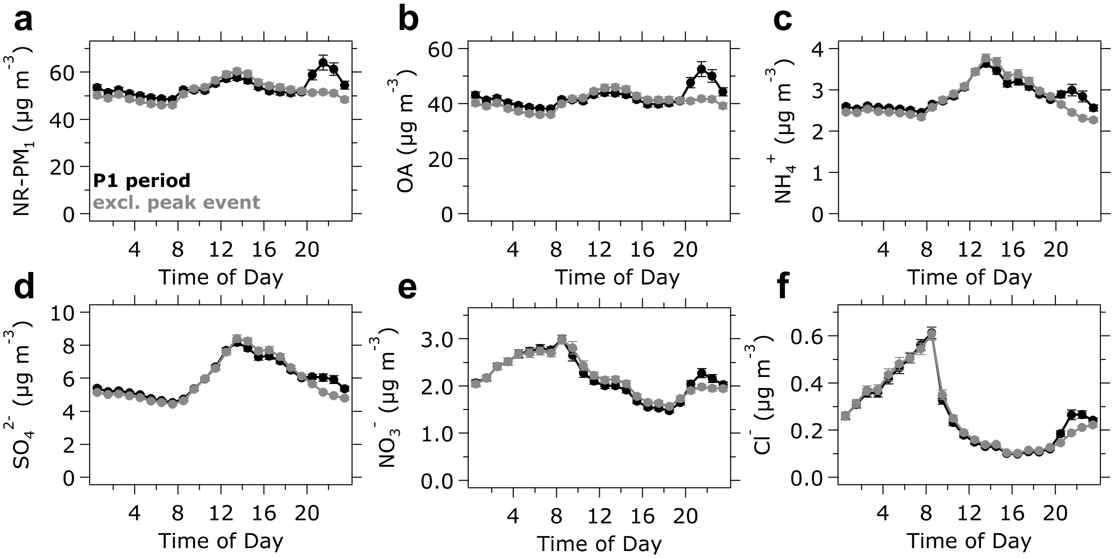

Figure S9: Diurnal variations of NR-PM$_1$, OA, and inorganic compounds during P1 period (black lines). Grey lines show the diurnal variations during P1 period without the peak event on October 19-20. The peak event notably influenced the night peak (20:00-00:00) of all OA factors.

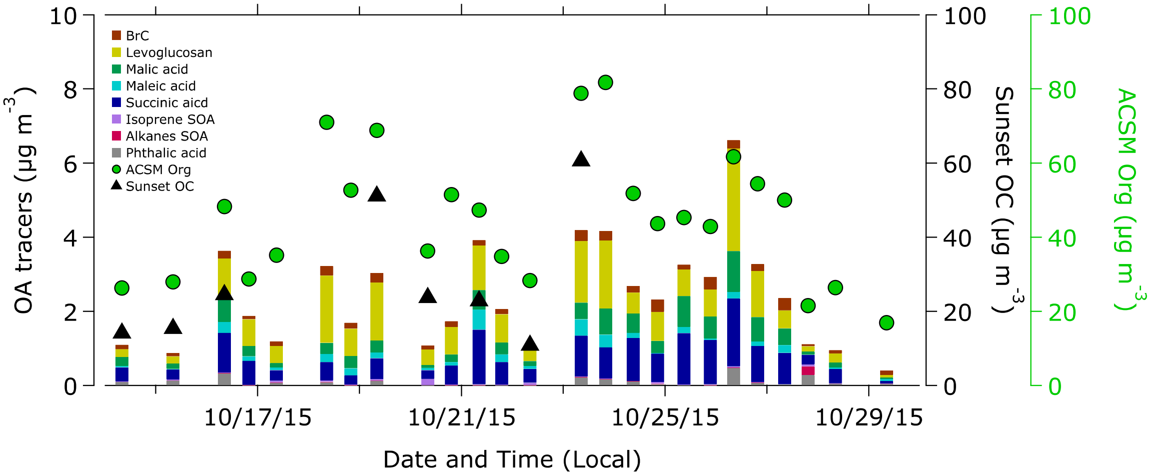

Figure S10: Sum of OA tracers quantified from integrated samples (left y-axis). Right axes show OC and OA measured by Sunset instrument and ToF-ACSM, respectively.

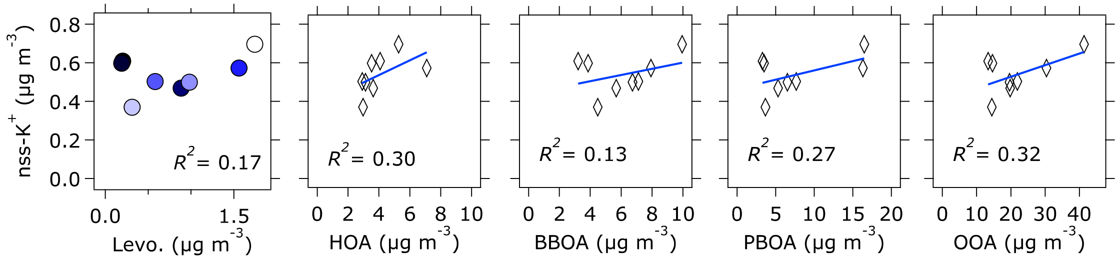

Figure S11: Linear regressions of non-sea-salt K^+ versus levoglucosan from integrated filter samples and OA factors from ME-2 analysis.

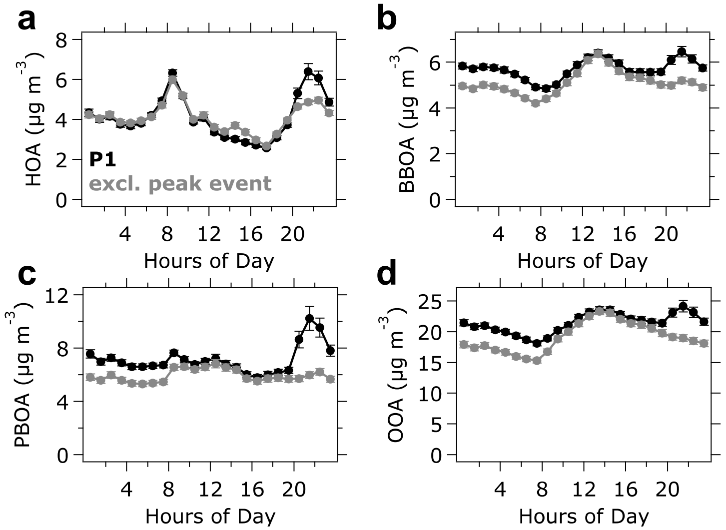

5 **Figure S12: Diurnal variations of the OA factors during P1 period (black lines). Grey lines show the diurnal variations during P1 period without the peak event on October 19-20. The peak event notably influenced the night peak (20:00-00:00) of all OA factors.**

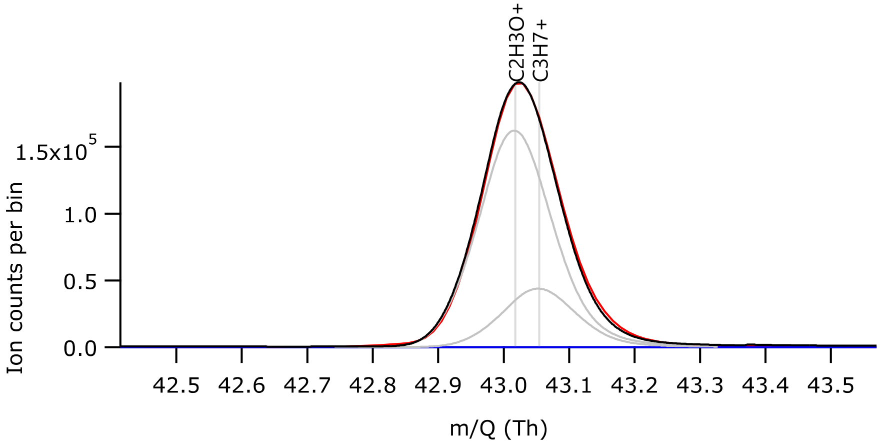

Figure S13: Peak fitting of *m/z* 43.

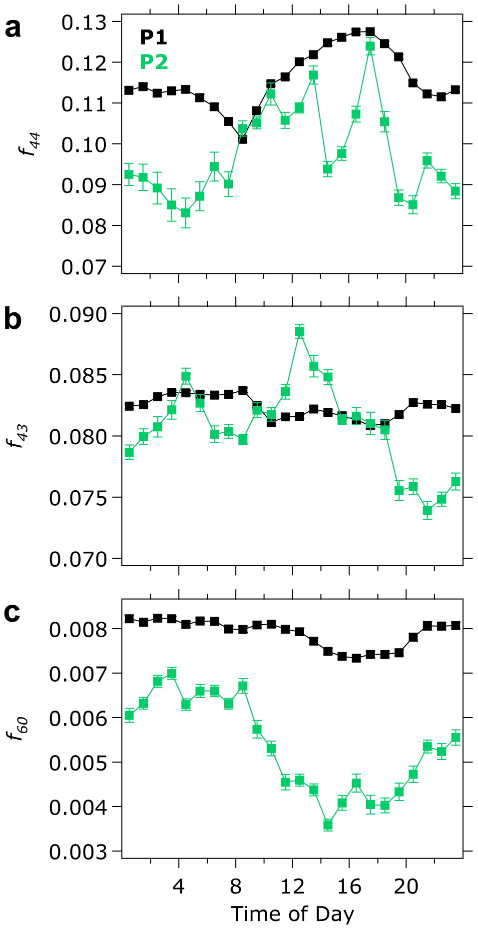

Figure S14: Diurnal variations of (a) f_{44}, (b) f_{43}, and (c) f_{60} for P1 and P2 periods.

References

Budisulistiorini, S. H., Canagaratna, M. R., Croteau, P. L., Marth, W. J., Baumann, K., Edgerton, E. S., Shaw, S. L., Knipping, E. M., Worsnop, D. R., Jayne, J. T., Gold, A. and Surratt, J. D.: Real-time continuous characterization of secondary organic aerosol derived from isoprene epoxydiols in downtown Atlanta, Georgia, using the Aerodyne Aerosol Chemical Speciation Monitor, Environ. Sci. Technol., 47(11), 5686–5694, doi:10.1021/es400023n, 2013.

Budisulistiorini, S. H., Li, X., Bairai, S. T., Renfro, J., Liu, Y., Liu, Y. J., McKinney, K. A., Martin, S. T., McNeill, V. F., Pye, H. O. T., Nenes, A., Neff, M. E., Stone, E. A., Mueller, S., Knote, C., Shaw, S. L., Zhang, Z., Gold, A. and Surratt, J. D.: Examining the effects of anthropogenic emissions on isoprene-derived secondary organic aerosol formation during the 2013 Southern Oxidant and Aerosol Study (SOAS) at the Look Rock, Tennessee, ground site, Atmos. Chem. Phys., 15(15), 8871–8888, doi:10.5194/acp-15-8871-2015, 2015.

Budisulistiorini, S. H., Baumann, K., Edgerton, E. S., Bairai, S. T., Mueller, S., Shaw, S. L., Knipping, E. M., Gold, A. and

Surratt, J. D.: Seasonal characterization of submicron aerosol chemical composition and organic aerosol sources in the southeastern United States: Atlanta, Georgia,and Look Rock, Tennessee, Atmos. Chem. Phys., 16(8), 5171–5189, doi:10.5194/acp-16-5171-2016, 2016.

Budisulistiorini, S. H., Riva, M., Williams, M., Chen, J., Itoh, M., Surratt, J. D. and Kuwata, M.: Light-absorbing brown carbon aerosol constituents from combustion of Indonesian peat and biomass, Environ. Sci. Technol., 51(8), 4415–4423, doi:10.1021/acs.est.7b00397, 2017.

Cheng, Y., Engling, G., He, K.-B., Duan, F.-K., Ma, Y.-L., Du, Z.-Y., Liu, J.-M., Zheng, M. and Weber, R. J.: Biomass burning contribution to Beijing aerosol, Atmos. Chem. Phys., 13(15), 7765–7781, doi:10.5194/acp-13-7765-2013, 2013.

Crippa, M., DeCarlo, P. F., Slowik, J. G., Mohr, C., Heringa, M. F., Chirico, R., Poulain, L., Freutel, F., Sciare, J., Cozic, J., Di Marco, C. F., Elsasser, M., Nicolas, J. B., Marchand, N., Abidi, E., Wiedensohler, A., Drewnick, F., Schneider, J., Borrmann, S., Nemitz, E., Zimmermann, R., Jaffrezo, J.-L., Pr'ev\^ot, A. S. H. and Baltensperger, U.: Wintertime aerosol chemical composition and source apportionment of the organic fraction in the metropolitan area of Paris, Atmos. Chem. Phys., 13(2), 961–981, doi:10.5194/acp-13-961-2013, 2013.

Crippa, M., Canonaco, F., Lanz, V. A., Äijälä, M., Allan, J. D., Carbone, S., Capes, G., Ceburnis, D., Dall'Osto, M., Day, D. A., DeCarlo, P. F., Ehn, M., Eriksson, A., Freney, E., Hildebrandt Ruiz, L., Hillamo, R., Jimenez, J. L., Junninen, H., Kiendler-Scharr, A., Kortelainen, A.-M., Kulmala, M., Laaksonen, A., Mensah, A. A., Mohr, C., Nemitz, E., O'Dowd, C., Ovadnevaite, J., Pandis, S. N., Petäjä, T., Poulain, L., Saarikoski, S., Sellegri, K., Swietlicki, E., Tiitta, P., Worsnop, D. R., Baltensperger, U. and Prévôt, A. S. H.: Organic aerosol components derived from 25 AMS data sets across Europe using a consistent ME-2 based source apportionment approach, Atmos. Chem. Phys., 14(12), 6159–6176, doi:10.5194/acp-14-6159-2014, 2014.

Fountoukis, C. and Nenes, A.: ISORROPIA II: a computationally efficient thermodynamic equilibrium model for K^+–Ca^{2+}–Mg^{2+}–NH_4^+–Na^+–SO_4^{2-}–NO_3^-–Cl^-–H_2O aerosols, Atmos. Chem. Phys., 7(17), 4639–4659, doi:10.5194/acp-7-4639-2007, 2007.

Ma, Y., Xu, X., Song, W., Geng, F. and Wang, L.: Seasonal and diurnal variations of particulate organosulfates in urban Shanghai, China, Atmos. Environ., 85(Supplement C), 152–160, doi:https://doi.org/10.1016/j.atmosenv.2013.12.017, 2014.

Ng, N. L., Canagaratna, M. R., Jimenez, J. L., Zhang, Q., Ulbrich, I. M. and Worsnop, D. R.: Real-time methods for estimating organic component mass concentrations from aerosol mass spectrometer data, Environ. Sci. Technol., 45(3), 910–916, doi:10.1021/es102951k, 2011.

Riva, M., Budisulistiorini, S. H., Chen, Y., Zhang, Z., D'Ambro, E. L., Zhang, X., Gold, A., Turpin, B. J., Thornton, J. A., Canagaratna, M. R. and Surratt, J. D.: Chemical characterization of secondary organic aerosol from oxidation of isoprene hydroxyhydroperoxides, Environ. Sci. Technol., 50(18), 9889–9899, doi:10.1021/acs.est.6b02511, 2016.

Robinson, N. H., Newton, H. M., Allan, J. D., Irwin, M., Hamilton, J. F., Flynn, M., Bower, K. N., Williams, P. I., Mills, G., Reeves, C. E., McFiggans, G. and Coe, H.: Source attribution of Bornean air masses by back trajectory analysis during the OP3 project, Atmos. Chem. Phys., 11(5), 9605–9630, doi:10.5194/acp-11-9605-2011, 2011.

Simoneit, B. R. T., Schauer, J. J., Nolte, C. G., Oros, D. R., Elias, V. O., Fraser, M. P., Rogge, W. F. and Cass, G. R.: Levoglucosan, a tracer for cellulose in biomass burning and atmospheric particles, Atmos. Environ., 33(2), 173–182, doi:10.1016/S1352-2310(98)00145-9, 1999.

Surratt, J. D., Kroll, J. H., Kleindienst, T. E., Edney, E. O., Claeys, M., Sorooshian, A., Ng, N. L., Offenberg, J. H., Lewandowski, M., Jaoui, M., Flagan, R. C. and Seinfeld, J. H.: Evidence for organosulfates in secondary organic aerosol, Environ. Sci. Technol., 41(2), 517–527, doi:10.1021/es062081q, 2007.

Zhang, Q., Jimenez, J. L., Worsnop, D. R. and Canagaratna, M.: A case study of urban particle acidity and its influence on secondary organic aerosol, Environ. Sci. Technol., 41(9), 3213–3219, doi:10.1021/es061812j, 2007.